Hybrid femtocell–attocell optical links for indoor free-space optical communication

Spencer Liverman
Siyuan Chen
Arun Natarajan
Alan X. Wang

Hybrid femtocell–attocell optical links for indoor free-space optical communication

Spencer Liverman, Siyuan Chen, Arun Natarajan, and Alan X. Wang*
Oregon State University, School of Electrical Engineering and Computer Science, Corvallis, Oregon, United States

Abstract. The demand for wireless bandwidth is increasing rapidly; however, the throughput of short-range radio frequency (RF) solutions, such as WiFi, are quickly reaching limits due to limited bandwidth in the RF spectrum. This problem can be overcome by utilizing unregulated infrared wavelengths in the optical spectrum. On the other hand, free-space optical (FSO) communication presents a challenge for mobility due to the line-of-sight nature of optics. We present a dual-channel optical link for short-range FSO communication, which consists of a 100 Mb/s, large diameter (60 cm at 3 m distance) optical femtocell with a 1.5 Gb/s, small diameter (1 cm at 3 m distance) optical attocell embedded within the femtocell. This hybrid femtocell–attocell optical link addresses the needs of various users by providing a high mobility femtocell link combined with an enhanced bandwidth attocell hotspot. A prototype hybrid system was assembled and evaluated in terms of bandwidth, range, and bit error rate (BER). In addition, the relationship between the incident angle of the transmitted beam relative to the receiver and the BER of the received data was evaluated. At a communication distance of 3 m, the BER is $<10^{-4}$ when the incident angle is smaller than 30 deg for the optical femtocell, while the incident angle must be smaller than 10 deg for the optical attocell to achieve the same level of BER. In addition, we experimentally demonstrated simultaneous, error-free recovery of the data from both the femtocell and the attocell when these two cells are overlapped, which proves the feasibility of the dual-channel optical link for FSO communication. © 2019 Society of Photo-Optical Instrumentation Engineers (SPIE) [DOI: 10.1117/1.OE.58.8.086112]

Keywords: optical communication networks; free-space optical communications; wireless communications; electro-optic modulation; lasers.

Paper 190634 received May 11, 2019; accepted for publication Aug. 1, 2019; published online Aug. 27, 2019.

1 Introduction

Wireless data traffic is currently increasing at an exponential rate worldwide with no sign of slowing down. If this trend continues, current radio frequency (RF) technologies will struggle to keep up with demand. The RF spectrum that is currently available for commercial use is limited to narrowbands centered around 2.4 and 5 GHz, which places an inherent limitation on the total achievable bandwidth of existing systems. In addition, RF signals have specific characteristics that limit how densely wireless access points (APs) can be grouped together, such as their ability to broadcast over large areas and penetrate through walls.

Recently, free-space optical (FSO) links have been suggested as an alternative to RF technologies.[1–10] Unlike RF signals, FSO channels are line-of-sight (LOS) links that do not penetrate through walls and can be packed into high-density femtocells or even ultrahigh-density attocells.[11–14] Utilizing FSO links to reduce the size of the wireless cell dramatically increases the bandwidth available to each end user by reducing the number of users on a single link. FSO links also create a physical layer of protection by necessitating that each user be placed directly under the transmitting light source.[15] One unresolved challenge in implementing an effective FSO system is the establishment of the uplink. To resolve this issue, hybrid femtocell networks involving both FSO and RF technologies have been suggested.[16–25] In these systems, the downlink that supports the bulk of data transfer would be established through an FSO channel, and the uplink, which mainly requests information, would be established via a pre-existing RF channel. The RF link would also create an effective feedback mechanism, which can enable dynamic load balancing and seamless hand-offs between FSO transmitters.[26–30] In addition to the work that has been completed for short-range hybrid links, recent analysis has shown that receiver diversity can improve the signal-to-noise ratio (SNR) of signals that have been degraded by atmospheric turbulence and pointing errors.[31–34] Two hop-relay-assisted systems that utilize optical links as a backhaul mechanism and RF links as a short-range link to the end user have also been proposed.[35]

Regardless of the arrangement or orientation, the key constraint when designing an effective optical communication system is the size of the optical cell. If the optical cells are too small, a large working area would require an unreasonable number of optical cells and would reduce the mobility within each cell. In addition, there is a trade-off between power density and bandwidth. Therefore, the size of the optical cells in FSO systems must be carefully designed to balance the requirement of bandwidth, mobility, and user coverage.

We propose a dual-channel FSO transmitter, in which a high-speed optical attocell is placed within a medium-speed optical femtocell. This architecture provides a solution to the bandwidth versus mobility problem by implementing two overlapping links, which have each been optimized for a specific purpose. The femtocell link provides mobility and moderate bandwidth, while the attocell link provides an LOS

hotspot with superior bandwidth. The parallel link approach presented in this paper offers a practical and effective means of overcoming a fundamental and persistent problem in the field of FSO communications. The remainder of this paper is organized as follows. In Sec. 2, we present our hybrid femtocell–attocell optical link and discuss its components in detail. In Sec. 3, the hybrid femtocell–attocell optical link is evaluated in terms of bandwidth, range, and bit error rate (BER). Section 4 concludes this paper.

2 Hybrid Femtocell–Attocell Optical Links

When designing an FSO communication link, one of the fundamental questions that must be addressed is how to determine the divergent angle of the transmitting light source since there is a trade-off between the coverage area and the power density at the receiver. The second trade-off that must be considered is between power and bandwidth. Increasing the power output of an FSO transmitter is clearly advantageous for improving the SNR in the link; however, doing so also tends to reduce the bandwidth of the transmitter proportionally. This issue is apparent in visual light communication (VLC) systems, which tend to broadcast optical signals over a large area. VLC systems offer improved mobility but must rely on sophisticated modulation methods to compete with the bandwidth capabilities of radially available WiFi routers. When considered together, four parameters (received power density, mobility, power output, and bandwidth) define the constraints in the design of an FSO link.

Optimization of the four parameters listed above depends heavily on the requirement of the end user. The commercial success of any indoor FSO link will depend heavily on its ability to compete with the already well-established WiFi links. If the solid angle of the transmitted light cone can be set to a reasonably large value, limited mobility can be achieved under each passive transmitter. Mobility in the greater FSO network can be expanded by packing multiple transmitters into a workspace, as shown in Fig. 1(a), and through the implementation of a simple hand-off mechanism.

In Fig. 1(a), the Gaussian-shape femtocell optical profile is shown is red while the much smaller attocell profile is represented as a black dot. The distance d between the optical femtocells is determined by the power density within the

femtocell and the sensitivity of the receiver. The honeycomb packing pattern, as shown in Fig. 1(a), allows for optimal transmitter density. In the design of our hybrid femtocell–attocell FSO system, we will balance the needs of all users by implementing a system in which two overlapping FSO channels are available in each optical cell. The first channel will serve as a medium-speed 100 Mb/s link operating at 980 nm and will offer moderate mobility to the end user, while the second channel operating at 850 nm serves as a purely LOS high-speed 1.5 Gb/s link. These two channels will be referred to as femtocells and attocells, respectively. The respective wavelengths for each cell are selected in the near-infrared to match the peak sensitivity of off-the-shelf silicon photodiodes. The separation between the two wavelengths is designed to ensure that both channels can be operated simultaneously while overlapping. On the receiving end, a narrowband optical filter will be used for the high-speed channel so that the lower power 1.5 Gb/s signal can be distinguished from the higher power 100 Mb/s signal. Figure 1(b) shows a side-view profile of the dual-channel system described above. In Fig. 1(b), θ is the divergent angle of the transmitted beam, h is the vertical distance between a given FSO transmitter and the receiver pair, and d is the lateral distance between FSO transmitters. Typical values of θ are 6 deg for the optical femtocell and 0.2 deg for the attocell. The distance h has a maximum value of 3 m and the distance d is roughly 60 cm.

2.1 Femtocell Design

In our FSO system, the 980-nm wavelength femtocell serves as the primary data link between the AP and the end user. The design of this optical cell will allow the users to stream data at speeds of up to 100 Mb/s without having to carefully align their receivers with the transmitted beam. A 200-mW side-emitting Fabry–Pérot (FP) laser diode was chosen as the transmitting light source for this link. An analog driver utilizing a passive RF-matching network and an enhanced-mode pseudomorphic high-electron-mobility transistor (E-pHEMT) was designed to drive the FP laser diode. E-pHEMT transistors have previously been used in RF wireless transmitter applications because of their capacity for substantial drain currents and large bandwidths. An adjustable aspheric collimating lens was paired with the FP laser

(a)   (b)
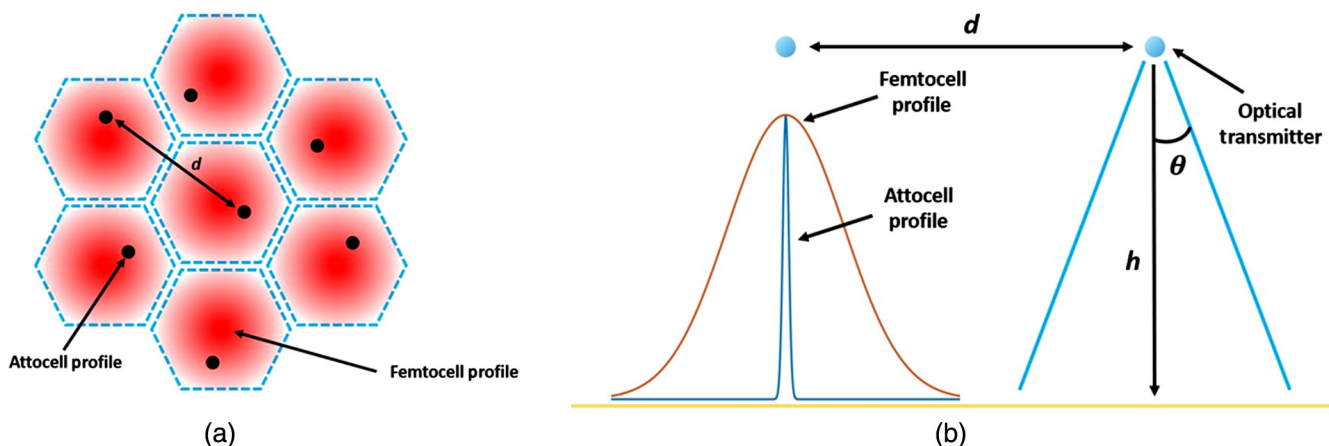
Fig. 1 Overlapping FSO femtocell and attocell profiles: (a) top view with honeycomb AP packing and (b) side view with design constraints.
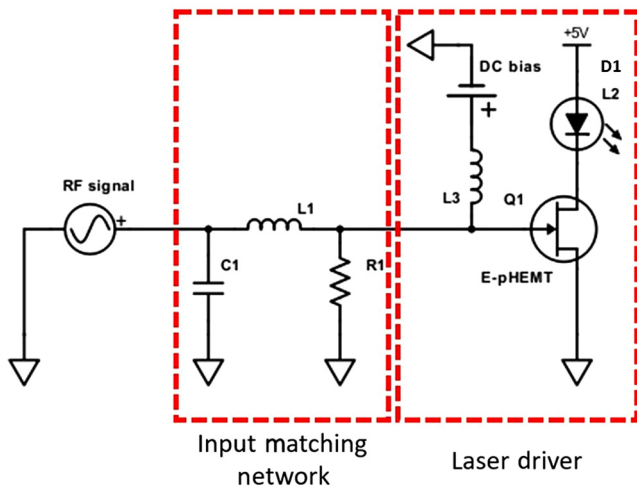
Fig. 2 Laser driver schematic representation used for both the femtocell and the attocell transmitters.

Fig. 3 FSO transmitter PCBs showing the femtocell and attocell transmitters mounted to a 3-m optical rail.

diode so that the divergent angle of the transmitter could be adjusted to a desired value. The schematic of the FP laser driver design is shown in Fig. 2. The same general driver design is also used to drive the vertical-cavity surface-emitting laser (VCSEL) diode in the FSO attocell; however, several of the component values were modified in that design to better suit the low-power VCSEL. The component values used in the femtocell design are shown below in Table 1.

To balance the trade-off between power density and mobility, the divergent angle of the optical femtocell was set to 6 deg. In a standard office environment, the distance between the ceiling and the surface of a desk is 3 m; therefore, the diameter of the femtocell light cone at the receiver is roughly 60 cm. A working spot size diameter of 60 cm is large enough that a given user can place their computer anywhere on a normal size desk and still receive a strong signal, while also small enough to ensure that the user does not have to share that connection with an adjacent user.

2.2 Attocell Design

The 850-nm wavelength attocell in our FSO system has been designed to optimize bandwidth for applications that demand higher data throughputs. The attocell link will give users access to data rates of up to 1.5 Gb/s; however, that increase in bandwidth comes at the cost of mobility. For the attocell link, a 2-mW VCSEL diode was selected as the transmitting

light source due to its high quantum efficiency and large bandwidth. VCSELs have also been widely adopted in the telecom industry because they are highly reliable and can be purchased at low cost. These traits also make them very attractive for FSO communication; however, the power output of these devices is very limited. Subsequently, the divergent angle of an FSO transmitter utilizing a VCSEL diode needs to be reduced to achieve enough power density. The resulting beam is highly collimated and LOS by nature. To gain access to the attocell link, a user would have to place their receiver directly under the attocell transmitter hotspot and would not be free to move the receiver until they no longer require the high-speed link. However, when the receiver is placed within the attocell hotspot, the user would have access to a link more than 10× faster than that of the optical femtocell.

A different E-pHEMT was chosen to better match the current and bandwidth requirements of the VCSEL diode. In addition, the component values used in the RF-matching network were redesigned to provide a better match at higher frequencies. An aspheric lens was also attached to the attocell transmitter to collimate the transmitted beam. The goal of this lens is to maximize the power density at the receiver by reducing the solid angle of the transmitted beam as much as possible. Figure 3 shows the schematic representation of the attocell transmitter with the component values listed below in Table 2.

Table 1 Femtocell transmitter components.

Schematic symbol	Description of FSO transmitter components	Part number/value
C1	Matching capacitor	4 pF
L1	Matching inductor	8.2 nH
R1	Matching resistor	50 Ω
L2	RF choke	7 μH
D1	FP laser diode	L980P200
HEMT	Driving transistor	ATF11P8

Table 2 Attocell transmitter components.

Schematic symbol	Description of FSO transmitter components	Part number/value
C1	Matching capacitor	2.4 pF
L1	Matching inductor	4 nH
R1	Matching resistor	50 Ω
L2	RF choke	7 μH
D1	VCSEL diode	HFE4093-342
HEMT	Driving transistor	ATF531P8

In our experimental setup, both the femtocell and the attocell transmitter printed circuit boards (PCBs) were mounted on a horizontal optical rail with the attocell transmitter placed under the femtocell to avoid blocking the optical path. Both transmitter boards look identical with the exception of an additional lens placed in front of the attocell transmitter. This lens is used to further focus the attocell beam on the receiver board. A picture of both transmitter PCBs is shown in Fig. 3.

2.3 Optical Receiver Design

The FSO receiver in our system must be capable of receiving signals from both the femtocell and the attocell transmitters simultaneously. To achieve this, two different photodiodes will be incorporated into the final receiver design. The size of each photodiode was chosen to satisfy the specific design constraints of each link. For the femtocell link, a large area p-type, intrinsic, n-type diode (PIN) diode with an encapsulated plastic lens was selected to maximize received optical power. The femtocell link transmitter has a relatively high-power output and limited bandwidth, which makes an inexpensive PIN diode a natural choice. However, the bandwidth and sensitivity requirements for the attocell link are much higher. Even after collimation, the power density in the attocell beam is smaller than that of the femtocell beam and the bandwidth is much higher. Therefore, the active area of the receiving photodiode must be smaller. To overcome these challenges, a small, low capacitance photodiode was chosen for the attocell design. Another issue to consider is the overlap between the femtocell and the attocell links. This problem is solved by placing a 40-nm full width at half maximum (FWHM) optical filter with a center wavelength of 850 nm in front of the attocell PIN. The optical filter paired with the attocell's PIN diode will reduce the interference from the 980-nm input light in the femtocell link substantially. For the femtocell link, the frequency of the signal emitted from the attocell transmitter is well above the cutoff frequency of the large area PIN diode and will simply be filtered out if a user accessing the femtocell link walks directly under the attocell beam. This arrangement will allow both links to work simultaneously even when the transmitted beams of each link overlap.

The analog front end for the high-speed and low-speed photodiodes will be almost identical; however, the bandwidth of the amplifiers used in each data path will be adjusted to match the bandwidth of each photodiode. In this system, a simple non-return-to-zero on-off-keying modulation scheme was selected to minimize the complexity and maximize the SNR. As a result, the analog front end will maximize sensitivity by saturating the received signal. First, the received optical signal will be converted into a voltage through a transimpedance amplifier (TIA). The recovered signal will be amplified by a linear amplifier and then saturated by a limiting amplifier (LA). The saturated signal will then be sent to a clock-data recovery (CDR) circuit. In an effort to keep the prototype design of the receiver as modular as possible, the femtocell and attocell components were placed on two separate PCBs. In a later version of the project, the two receiving components will be placed on a single PCB. Figure 4(a) shows a schematic representation detailing the receiver components for both the low-speed and high-speed links, while Fig. 4(b) shows pictures of the femtocell and attocell receivers mounted to the same secondary optical rail. This small 0.5-m optical rail is mounted perpendicularly to the larger 3-m optical rail and will be used to vary the lateral position of the femtocell and attocell receivers. For continuity, locations on the larger 3-m optical rail will be referred to as vertical positions and locations on the smaller 0.5-m perpendicular rail will be referred to as lateral positions. Tables 3 and 4 detail the specific components used in the femtocell and attocell receivers, respectively.
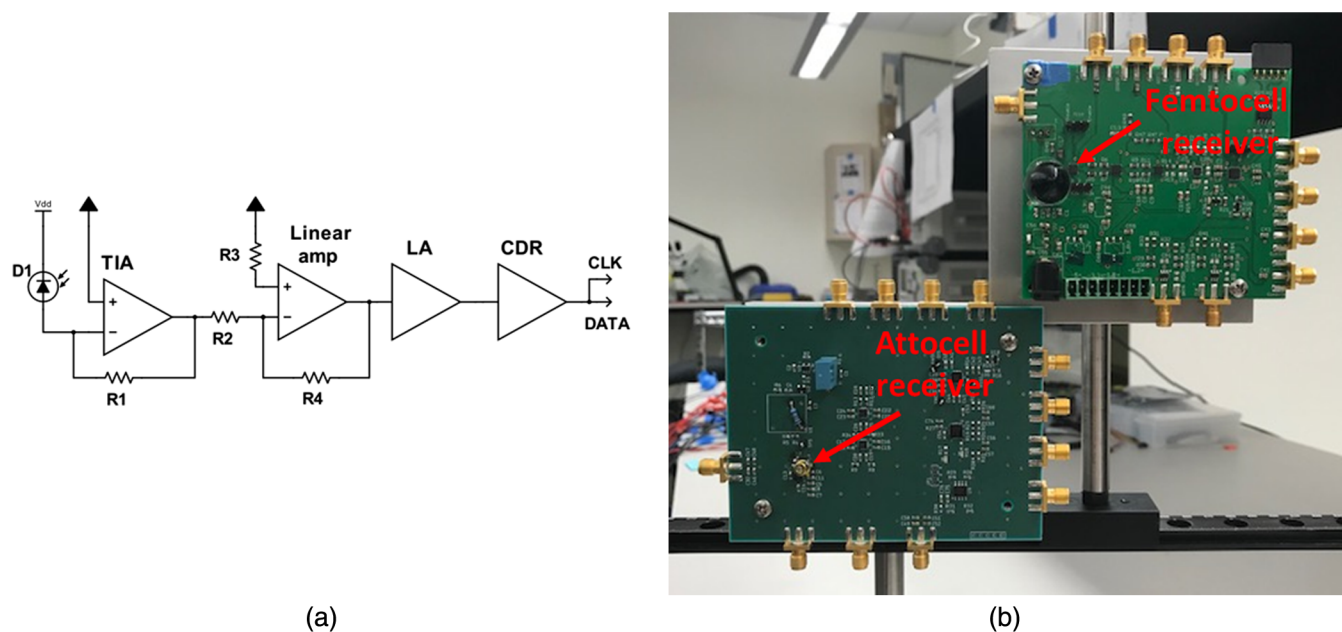
Fig. 4 Dual-channel FSO receiver: (a) schematic representation of both the femtocell and attocell receivers, (b) femtocell and attocell receivers mounted to the 0.5-m lateral optical rail.

Table 3 Femtocell receiver components.

Schematic symbol	Description of FSO receiver components	Part number
D1	Photodiode	S6968-01
TIA	Transimpedance amplifier	OPA857
Linear	Linear amplifier	THS4541
LA	Limiting amplifier	ADN2890
CDR	Clock-data recovery circuit	ADN2915

Table 4 Attocell receiver components.

Schematic symbol	Description of FSO receiver components	Part number
D1	Photodiode	S5971
TIA	Transimpedance amplifier	HMC799
Linear	Linear amplifier	LTC6401
LA	Limiting amplifier	HMC914
CDR	Clock-data recovery circuit	ADN2813

3 Hybrid Femtocell–Attocell Link Evaluation

The evaluation of our dual-channel FSO communication system requires the evaluation of the femtocell and attocell links individually and the evaluation of both links operating simultaneously. The success of our system requires that each link performs adequately as a stand-alone connection and that both links also perform well simultaneously while overlapping. To demonstrate this experimentally, the femtocell and attocell links will first be tested without the presence of the other link. After those tests are complete, both links will be switched on at the same time. The results from each set of tests will then be reviewed to determine the effectiveness of our dual-channel configuration. In each of these tests, the parameters of interest will include the vertical distance

between the transmitter and the receiver, the lateral distance between the receiver and the optical axis, and relative incident angle between the receiver and the optical axis. The metric that we will use to evaluate the performance of our system is the BER. Figure 5(a) shows a diagram outlining the test parameters described above.

The BER tests performed during the evaluation of this FSO communication system will all follow the same general procedure. First, a bit error rate testing (BERT) scope will generate a pseudorandom bit sequence (PRBS). That sequence will serve as an input for a given transmitter under test, which will then transmit the PRBS signal across the optical channel. The receiver that corresponds to the transmitter under test will then recover the transmitted signal and send it back to the BERT scope. Lastly, the BERT scope will compare the transmitted and recovered signals and calculate a BER. A block diagram detailing the main components of this test setup is shown in Fig. 5(b) and a photo of the test setup is shown in Fig. 5(c). In the case of the final test in which both the femtocell and the attocell are active at the same time, two different PRBS signals will be used simultaneously. The BERT scope is only capable of outputting one unique signal at a time, so an arbitrary waveform generator (AWG) will be used to produce the second signal. The eye diagrams for both signals can then be captured simultaneously on an oscilloscope.

3.1 Femtocell Performance Evaluation

In our FSO communication system, an optical femtocell will provide the main channel over which data are transferred. The goal in the design of this link is to cover as large an area as possible while still maintaining a sufficiently low BER. In this evaluation, a BER of 10^{-4} will be used as a benchmark value. When the BER in a communication system drops below 10^{-4}, simple forward error correction (FEC) codes can be applied to further reduce the BER by 2 to 3 orders of magnitude using well-established Reed–Solomon codes. However, when the input BER rises above 10^{-4}, FEC codes have little or no effect on the output BER. Unless otherwise stated, the bit rate for all femtocell evaluations is set to 100 Mb/s.

Using the aspheric lens mounted to the femtocell transmitter PCB, the divergent angle of the femtocell beam was
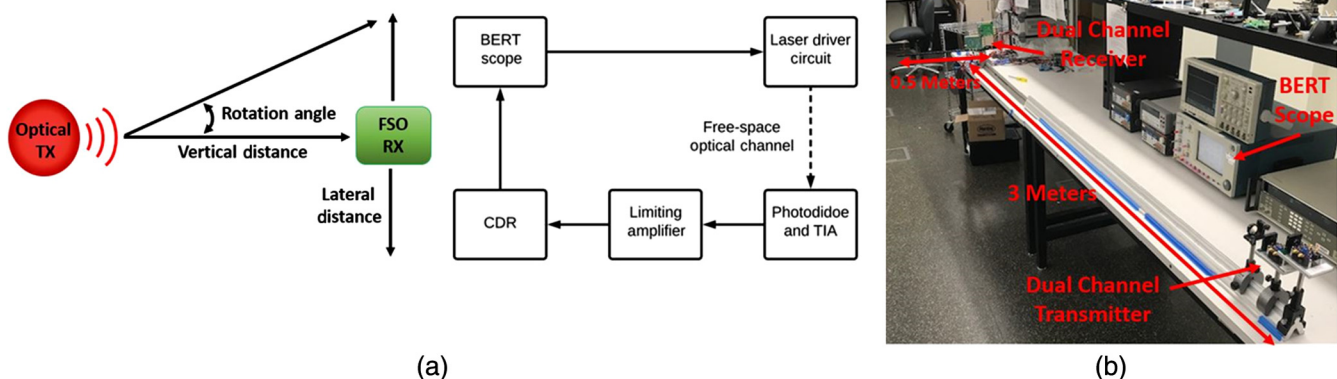
Fig. 5 FSO dual-channel test configuration: (a) diagram of relevant test parameters, (b) block diagram detailing the main components of the test setup, and (c) experimental test setup with 3-m vertical optical rail and 0.5-m lateral optical rail.
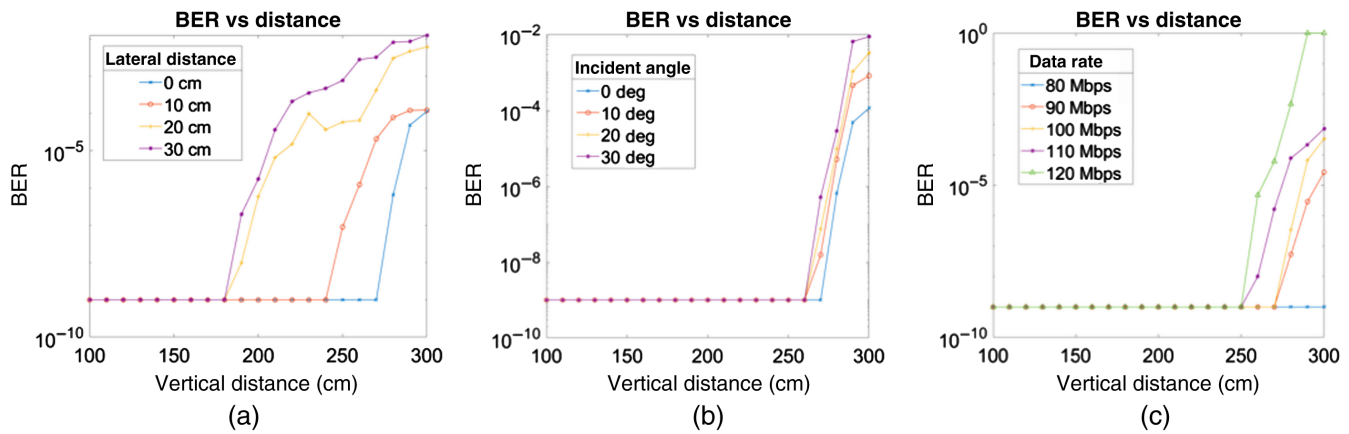
Fig. 6 Optical femtocell evaluation: (a) BER evaluation at various vertical and lateral distances, 100 Mb/s; (b) BER evaluation at various vertical distances and incident angles, 100 Mb/s; and (c) BER evaluation at various vertical distances and bit rates.

set to 6 deg. At a distance of 3 m, the resulting beam casts a light spot with a 60-cm diameter allowing for limited mobility within each optical cell. The relationship between vertical distance, lateral distance, and BER within a single optical femtocell is plotted in Fig. 6(a). When the femtocell receiver is placed within 10 cm of the optical axis, a BER rate of 10^{-4} is achieved for all vertical distances of 300 cm or less. However, when the lateral distance is increased to 20 cm, the BER exceeds 10^{-4} at a vertical distance of 270 cm and, at a lateral distance of 30 cm, the 10^{-4} cross point is 220 cm.

In addition to vertical and lateral distances, the relationship between BER and the incident angle was also evaluated. In a dynamic user environment, it is important to understand how varying the incident angle of the receiver will affect the BER. The results of this evaluation are plotted in Fig. 6(b). It is important to note that the viewing angle of the femtocell receiver is 30 deg, and for this evaluation, the femtocell receiver was placed directly on the optical axis. For vertical distances of <260 cm, angles up to 30 deg can be well tolerated. However, the BER increases above 10^{-4} for angles in the range of 10 deg to 30 deg at distances between 260 and 270 cm. The close grouping of the BER traces in Fig. 6(b) indicates that the relative change in BER is small for angular variations <30 deg.

The final stand-alone assessment that was completed for the femtocell link evaluates the effect of the link's bit rate on BER. The results of this evaluation are plotted in Fig. 6(c). At vertical distances of <250 cm, error-free transmission can be achieved for data rates of up to 120 Mb/s. The 10^{-4} cross point for data rates of 120 and 110 Mb/s are located at vertical distances of 240 and 250 cm, respectively. At a vertical distance of 300 cm, the BER for a data rate of 100 Mb/s does exceed 10^{-4} by a small margin. However, during previous tests, the BER was recorded as <10^{-4} at 100 Mb/s. This discrepancy can be attributed to small variations in the testing setup between tests. For data rates below 100 Mb/s, the BER is <10^{-4} for all distances <300 cm.

3.2 Attocell Performance Evaluation

The purpose of the optical attocell in our FSO communications system is to provide a high-speed link alternative to the optical femtocell for applications that demand high bandwidth connections. This link will utilize a much weaker

2-mW VCSEL diode which can be modulated at gigabit-per-second speeds. In addition, the wavelength of the attocell transmitter is blueshifted to 850 nm, which will allow for the addition of a bandpass optical filter on the receiving end. In this evaluation, a Thorlabs FBH850-40 bandpass optical filter with a center frequency of 850 nm and FWHM of 40 nm was used to filter out the 980-nm light transmitted from the femtocell link. Owing to the reduction in transmitted power, the solid angle of the attocell link must be drastically smaller than that of the femtocell link. At a distance of 300 cm, the diameter of the light spot cast by the attocell link is just 1 cm. This LOS link does not achieve significant mobility; however, it does provide a high bandwidth hotspot under which users can access gigabit-per-second data rates. In the following evaluations, the transmission date rate will be 1 Gb/s, unless otherwise stated.

To preserve power density within the attocell link, the transmitted beam is well collimated and therefore highly directional. Unlike the femtocell link, the attocell link does not experience a rapid loss of power density over distance. It is therefore not necessary to evaluate the BER of the link as a function of vertical and lateral distance. Owing to the collimated nature of the beam, the attocell link is very capable of transmitting over distances well in excess of 300 cm but cannot transmit to multiple lateral locations simultaneously. As a result, the first evaluation that will be considered is a relationship between the incident angle and BER. For this evaluation, the attocell receiver is placed on the optical axis relative to the attocell transmitter at a distance of 300 cm and is then rotated. The results of this evaluation are plotted in Fig. 7(a). Again, the benchmark for these evaluations will be 10^{-4}. From the plot in Fig. 7(a), it is clear that the attocell receiver can tolerate an angular variation of 10 deg. The limitation in angular tolerance can be attributed to the ball lens that is integrated in the transistor outline package of the high-speed PIN diode used in the attocell receiver design. This ball lens provides an important gain factor of about 4 but limits the viewing angle of the diode. Owing to the LOS nature of the attocell link, a viewing angle of 10 deg is more than sufficient for this design.

The second evaluation that was completed for the attocell link demonstrates the bandwidth potential of the link. For this evaluation, the attocell receiver was again placed at a
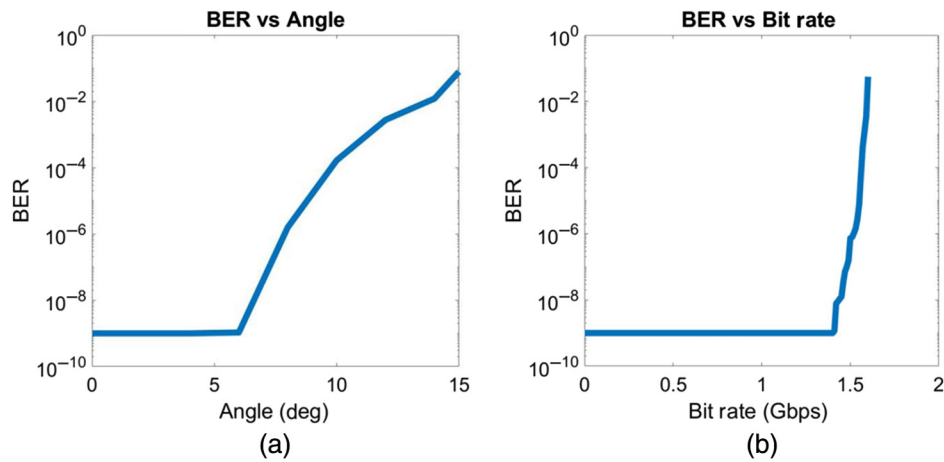
Fig. 7 Optical attocell evaluation: (a) BER evaluation at various incident angles and at a vertical distance of 300 cm, 1 Gb/s and (b) BER evaluation at various bit rates and at a vertical distance of 300 cm.

distance of 3 m and the relationship between the transmitted data rate and the BER was recorded. The results of that evaluation are plotted in Fig. 7(b). Error-free transmission was recorded for all data rates <1.4 Gb/s, and a maximum rate of 1.6 Gb/s was demonstrated while still maintaining a BER of $<10^{-4}$. These results show more than a 10× improvement over transmission speeds provided by the femtocell link. However, it is important to note again that this link is strictly LOS, with the attocell receiver placed directly in the path of the collimated attocell beam.

3.3 Dual-Channel System Evaluation

The final evaluation of our FSO communication system involves simultaneous recovery of both the femtocell and the attocell links. To ensure that this test reflects a realistic transmission scenario, the beam profiles of each link will overlap one another as much as possible. The signal integrity of the 200-mW 980-nm femtocell link is ensured via frequency filtering. Even if the attocell beam is incident on the femtocell receiver, the much higher-frequency components of that signal will be filtered out. The signal integrity of the 2-mW 850-nm attocell link will be ensured using the FBH850-40 bandpass filter mentioned previously. This arrangement allows both links to operate in the same area without signal interference.

The test setup for this evaluation is very similar to previous evaluations with the femtocell and attocell links placed 300-cm away from their respective receivers. The BERT scope used for previous evaluations was used to generate a 1-Gb/s attocell signal, while an AWG was used to generate a 100-Mb/s femtocell signal. On the receiving end, the outputs from both receivers were connected to an oscilloscope and the eye diagrams for each signal were captured. The results of this evaluation are shown in Fig. 8.

It is clear from Fig. 8 that the simultaneous recovery of both the femtocell and the attocell links is possible even when the profiles of both beams overlap. The strategies for
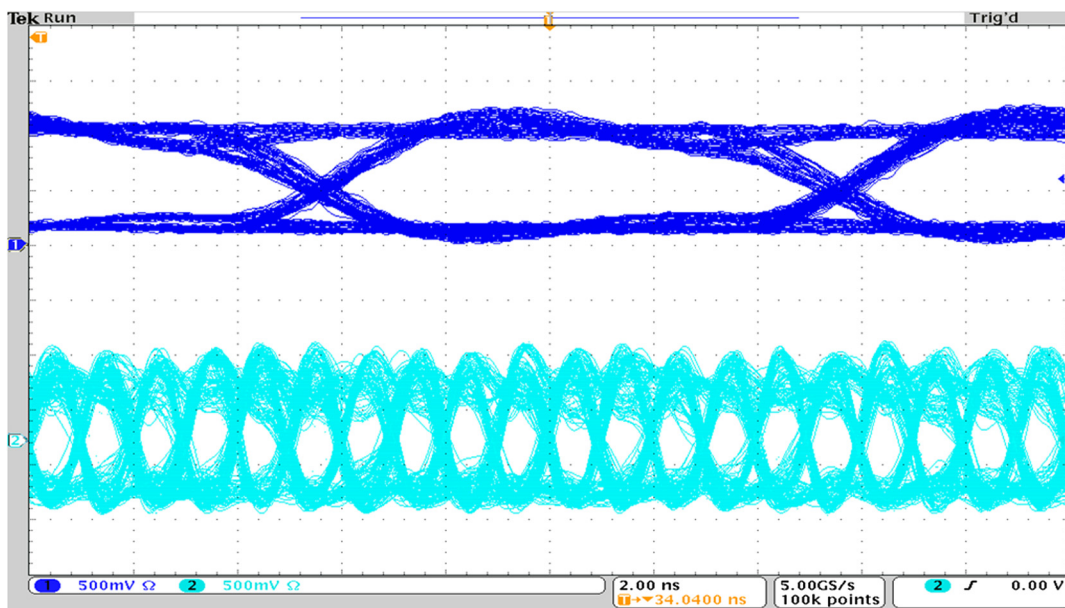
Fig. 8 Recovered eye diagrams for the femtocell (blue) and attocell (teal) links at data rates of 100 Mb/s and 1 Gb/s, respectively, over a distance of 300 cm.

mitigating intercell interference, which were described previously, were highly effective. Both eye diagrams exhibit open eye profiles and a peak-to-peak amplitude of ~1 V. The evaluation of the dual-channel optical communications system described in this paper was successful. In addition, the optical filters that are included in the design of the femtocell and attocell receivers make the system very robust against interface from ambient light sources. Any light incident on the femtocell receiver that is outside a 300-nm band centered on 850 nm is filtered out. The attocell receiver only receives light within a 40-nm band also centered around 850 nm.

4 Conclusion

In this paper, we have presented a hybrid femtocell–attocell FSO communication system. In this system, a dual-channel optical link architecture was designed, assembled, and evaluated based on range, angular tolerance, and BER performance. This system consists of a 60-cm diameter optical femtocell based on a 200-mW 980-nm FP laser diode, which is paired with a receiver achieving a 30 deg viewing angle and a 1-cm diameter optical attocell based on a 2-mW VCSEL diode, which is paired with a receiver achieving a 10 deg viewing angle. In this design, the optical attocell is located within the lager femtocell. Both cell diameters are measured at a distance of 300 cm. The femtocell link provides a 100-Mb/s link with moderate mobility, while the attocell link provides a 1.5-Gb/s LOS connection. Interference in the femtocell link was mitigated using frequency filtering, while interference in the attocell link was mitigated using optical filtering. In addition to demonstrating the potential of each link individually, we have also demonstrated the simultaneous recovery of both signals. Our experimental results have shown that this dual-channel, hybrid FSO system is an effective solution for providing users with both mobility-enabled medium-speed optical links and LOS high-speed optical links.

References

1. Z. Chen and H. Haas, "A simplified model for indoor optical attocell networks," in *IEEE Summer Top. Meeting Ser.*, pp. 167–168 (2015).
2. L. Feng et al., "Applying VLC in 5G networks: architectures and key technologies," *IEEE Network* **30**(6), 77–83 (2016).
3. A. Gupta, P. Garg, and N. Sharma, "Hybrid LiFi—WiFi indoor broadcasting system," in *IEEE 28th Annu. Int. Symp. Personal, Indoor, and Mob. Radio Commun.*, pp. 1–6 (2017).
4. D. Singh et al., "Design and implementation of wireless communication system for toll collection using LIFI," in *4th Int. Conf. Signal Process. Comput. and Control*, pp. 510–515 (2017).
5. J. O. Agyemang, J. J. Kponyo, and J. Mouzna, "Light fidelity (LiFi) as an alternative data transmission medium in VANET," in *Eur. Modell. Symp.*, pp. 213–217 (2017).
6. A. Surampudi, S. S. Chapalgaonkar, and P. Arumugam, "Can balloons produce Li-Fi? A disaster management perspective," in *Global LIFI Congr.*, pp. 1–5 (2018).
7. Z. P. Choudhari and S. R. Devane, "High sensitivity universal LiFi receiver for enhance data communication," in *Online Int. Conf. Green Eng. and Technol.*, pp. 1–5 (2016).
8. K. C. Hu et al., "Prototyping and measurements for a LiFi system," in *IEEE Sens. Array and Multichannel Signal Process. Workshop*, pp. 1–5 (2016).
9. H. Kazemi, M. Safari, and H. Haas, "Spectral efficient cooperative downlink transmission schemes for DCO-OFDM-based optical attocell networks," in *IEEE 84th Veh. Technol. Conf.*, pp. 1–6 (2016).
10. M. Zeng et al., "Design and demonstration of an indoor visible light communication network with dynamic user access and resource allocation," in *9th Int. Conf. Wireless Commun. and Signal Process.*, pp. 1–6 (2017).
11. C. Chen, D. A. Basnayaka, and H. Haas, "Downlink performance of optical attocell networks," *J. Lightwave Technol.* **34**(1), 137–156 (2016).
12. L. Yi and T. Cui, "Interference mitigation between femtocell and macrocell," in *Proc. 2011 Int. Conf. Electron. and Optoelectron.*, pp. V2-102–V2-104 (2011).
13. H. Kazemi and H. Haas, "Downlink cooperation with fractional frequency reuse in DCO-OFDMA optical attocell networks," in *IEEE Int. Conf. Commun.*, pp. 1–6 (2016).
14. C. Chen, D. Basnayaka, and H. Haas, "Downlink SINR statistics in OFDM-based optical attocell networks with a Poisson Point Process Network Model," in *IEEE Global Commun. Conf.*, pp. 1–6 (2015).
15. Z. Chen and H. Haas, "Physical layer security for optical attocell networks," in *IEEE Int. Conf. Commun.*, pp. 1–6 (2017).
16. I. S. Ansari et al., "A performance study of two hop transmission in mixed underlay RF and FSO fading channels," in *IEEE Wireless Commun. and Networking Conf.*, pp. 388–393 (2014).
17. I. S. Ansari et al., "Outage performance analysis of underlay cognitive RF and FSO wireless channels," in *3rd Int. Workshop in Opt. Wireless Commun.*, pp. 6–10 (2014).
18. I. Stefan, H. Burchardt, and H. Haas, "Area spectral efficiency performance comparison between VLC and RF femtocell networks," in *IEEE Int. Conf. Commun.*, pp. 3825–3829 (2013).
19. Q. Wang et al., "WiFO: a hybrid WiFi free-space optical communication networks of femtocells," in *MSWiM Conf.*, pp. 35–42 (2017).
20. N. Lorrière et al., "An OFDM testbed for LiFi performance characterization of photovoltaic modules," in *Global LIFI Congr.*, pp. 1–5 (2018).
21. M. R. H. Mondal and R. B. Faruque, "Hybrid diversity combined OFDM for LiFi," in *IEEE Int. Conf. Telecommun. and Photonics*, pp. 132–136 (2017).
22. H. Kazemi, M. Safari, and H. Haas, "A wireless backhaul solution using visible light communication for indoor Li-Fi attocell networks," in *IEEE Int. Conf. Commun.*, pp. 1–7 (2017).
23. S. Liverman et al., "Integrating free-space optical communication links with existing WiFi (WiFO) network," *Proc. SPIE* **9772**, 97720P (2015).
24. S. Liverman et al., "WiFO: a hybrid communication network based on integrated free-space optical and WiFi femtocells," *Comput. Commun.* **132**, 74–83 (2018).
25. Q. Wang, T. Nguyen, and A. X. Wang, "Channel capacity optimization for an integrated Wi-Fi and free-space communication system (WiFiFo)," in *Proc. 17th ACM Int. Conf. Model. Anal. and Simul. of Wireless and Mob. Syst.*, pp. 327–330 (2014).
26. M. D. Soltani et al., "Handover modeling for indoor Li-Fi cellular networks: the effects of receiver mobility and rotation," in *IEEE Wireless Commun. and Networking Conf.*, pp. 1–6 (2017).
27. Y. Wang, X. Wu, and H. Haas, "Fuzzy logic based dynamic handover scheme for indoor Li-Fi and RF hybrid network," in *IEEE Int. Conf. Commun.*, pp. 1–6 (2016).
28. Y. Wang and H. Haas, "Dynamic load balancing with handover in hybrid Li-Fi and Wi-Fi networks," *J. Lightwave Technol.* **33**(22), 4671–4682 (2015).
29. D. Nguyen-Huu, T. Duong, and T. Nguyen, "Location-assisted coding for FSO communication," *IEEE Trans. Commun.* **65**(10), 4360–4370 (2017).
30. M. D. Soltani et al., "Bidirectional user throughput maximization based on feedback reduction in LiFi networks," *IEEE Trans. Commun.* **66**, 3172–3186 (2018).
31. M. A. Amirabadi and V. T. Vakili, "A novel hybrid FSO/RF communication system with receive diversity," *Optik* **184**, 293–298 (2019).
32. M. A. Amirabadi and V. Tabataba Vakili, "A new optimization problem in FSO communication system," *IEEE Commun. Lett.* **22**(7), 1442–1445 (2019).
33. M. A. Amirabadi and V. T. Vakili, "Performance comparison of two novel relay-assisted hybrid FSO/RF communication systems," *IET Commun.* **13**, 1551–1556 (2019).
34. M. A. Amirabadi and V. T. Vakili, "Performance evaluation of a novel relay-assisted hybrid FSO/RF communication system with receive diversity," *IET Optoelectron.* (2019).
35. M. A. Amirabadi and V. T. Vakili, "On the performance of a multi-user multi-hop hybrid FSO/RF communication system," *Opt. Commun.* **444**, 172–183 (2019).

Spencer Liverman received his BSc degree in electrical engineering and computer science from Oregon State University (OSU) in 2014. He is currently enrolled at OSU as a PhD student and will graduate in June 2019. His graduate school research is focused on free-space optical (FSO) communications networks, analog circuit design, and system modeling. During his time at OSU, he has designed, implemented, and characterized several FSO communications systems for use in wireless indoor optical networks. He also served as the

principal investigator for an SBIR grant obtained by E-Lambda related to FSO links.

Siyuan Chen is an analog designer in OmniVision Technologies. She received her MS degree in electrical and computer engineering from OSU in 2018.

Arun Natarajan received his BTech degree from the Indian Institute of Technology, Madras, India, in 2001, and his MS and PhD degrees from the California Institute of Technology, Pasadena, California, USA, in 2003 and 2007, respectively, all in electrical engineering. From 2007 to 2012, he was a research staff member with IBM T. J. Watson Research Center, Yorktown Heights, New York, USA, and worked on millimeter-wave (mm-wave)-phased arrays for multi-Gb/s data links and airborne radar and on self-healing circuits for increased yield in submicron process technologies. In 2012, he joined OSU, Corvallis, Oregon, USA, where he is currently an associate professor in the School of EECS. His research is focused on radio frequency, mm-wave and sub-mm-wave-integrated circuits and systems for high-speed wireless communication and imaging.

Alan X. Wang is an associate professor at the School of Electrical Engineering and Computer Science in OSU. He received his BS degree from Tsinghua University, and his MS degree from the Institute of Semiconductors, Chinese Academy of Sciences, Beijing, China, in 2000 and 2003, respectively, and his PhD in electrical and computer engineering from the University of Texas at Austin in 2006. From January 2007 to August 2011, he was with Omega Optics, Inc., Austin, Texas, where he served as the chief research scientist for multiple government-funded Small Business Innovative Research projects. He joined OSU as an assistant professor in August 2011 and was promoted to associate professor in 2017. He is a senior member of the Institute of Electrical and Electronics Engineers (IEEE), the Optical Society of America (OSA), and SPIE.